Visualization of ribosome-recycling factor on the *Escherichia coli* 70S ribosome: Functional implications

Rajendra K. Agrawal*[†‡], Manjuli R. Sharma*, Michael C. Kiel[§], Go Hirokawa[§], Timothy M. Booth*, Christian M. T. Spahn[¶‖], Robert A. Grassucci[¶], Akira Kaji[§], and Joachim Frank[†¶]

*Wadsworth Center, New York State Department of Health, Empire State Plaza, Albany, NY 12201-0509; [†]Department of Biomedical Sciences, State University of New York, Albany, NY 12222; [§]Department of Microbiology, University of Pennsylvania School of Medicine, Philadelphia, PA 19104; and [¶]Howard Hughes Medical Institute, Health Research, Inc., Wadsworth Center, Empire State Plaza, Albany, NY 12201-0509

After the termination step of protein synthesis, a deacylated tRNA and mRNA remain associated with the ribosome. The ribosome-recycling factor (RRF), together with elongation factor G (EF-G), disassembles this posttermination complex into mRNA, tRNA, and the ribosome. We have obtained a three-dimensional cryo-electron microscopic map of a complex of the *Escherichia coli* 70S ribosome and RRF. We find that RRF interacts mainly with the segments of the large ribosomal subunit's (50S) rRNA helices that are involved in the formation of two central intersubunit bridges, B2a and B3. The binding of RRF induces considerable conformational changes in some of the functional domains of the ribosome. As compared to its binding position derived previously by hydroxyl radical probing study, we find that RRF binds further inside the intersubunit space of the ribosome such that the tip of its domain I is shifted (by ≈13 Å) toward protein L5 within the central protuberance of the 50S subunit, and domain II is oriented more toward the small ribosomal subunit (30S). Overlapping binding sites of RRF, EF-G, and the P-site tRNA suggest that the binding of EF-G would trigger the removal of deacylated tRNA from the P site by moving RRF toward the ribosomal E site, and subsequent removal of mRNA may be induced by a shift in the position of 16S rRNA helix 44, which harbors part of the mRNA.

Ribosomes are responsible for translating genetic information carried by mRNAs into specific sequences of amino acids. Translation on the ribosome comprises of four main steps: (*i*) initiation, (*ii*) elongation, (*iii*) termination, and (*iv*) recycling. Recent advancements in structural studies of the translational machinery have helped elucidate binding positions and functions of various translational factors involved in various stages of initiation (1, 2), elongation (3, 4), and termination (5–7). The fourth step of translation requires binding of a dedicated protein factor, the ribosome-recycling factor (RRF), which in conjunction with elongation factor G (EF-G) helps removing the mRNA and last deacylated tRNA from the ribosome (see ref. 8).

Atomic structures of RRF determined from five different species, including *Escherichia coli*, show that it is comprised of two structural domains: domain I, consisting of three long α-helix bundles, and the smaller domain II, which is an α/β motif (9–13). Different orientations of domain II in these structures have been attributed to interdomain flexibility, which is thought to be necessary for RRF to function on the ribosome (12).

The overall match in dimensions between RRF and tRNA (9) prompted the proposal of structural and functional molecular mimicry between the two molecules (9). In a recent study (14) using the hydroxyl radical probing (HRP) method, the orientation of RRF on the ribosome was derived. This study did not support the idea of direct molecular mimicry of tRNA by RRF, because the derived binding position of RRF was quite different from that one would expect based on structural mimicry. The inferred binding position of RRF overlaps with the binding positions of tRNA at both A and P sites, but in an orientation that puts the long axes of the two molecules in oblique directions. Here we present a three-dimensional cryo-electron microscopy

(cryo-EM) map of the *E. coli* 70S ribosome–RRF complex at 12-Å resolution (8.4 Å by 3σ criterion, see ref. 15). Our map directly shows a density attributable to RRF, in general agreement with the overall orientation of RRF inferred from the HRP study (14). The main difference is the fact that our study places RRF further (by ≈5 Å) inside the intersubunit space of the ribosome, with domain II of RRF being oriented more toward the 30S ribosomal subunit. In addition, the tip of domain I of RRF is shifted (by ≈13 Å) toward protein L5 of the 50S subunit. Furthermore, our study reveals important conformational changes of the ribosome upon binding of RRF, and lends further support to a previously proposed mechanism (16, 17) of RRF action for disassembly of the posttermination complex.

Materials and Methods

Preparation of the Ribosome–RRF Complex. The complex of the *E. coli* RRF and ribosome was prepared as described (16). Briefly, 96 pmol of 70S ribosomes and 220 pmol of RRF were incubated together for 10 min at room temperature in a total volume of 80 μl containing 52 mM Tris·HCl (pH 7.5), 25 mM KCl, 5.5 mM NH₄Cl, 11 mM Mg(OAc)₂, and 0.3 mM 2-mercaptoethanol. Occupancy of RRF on the ribosome, as estimated from the Western blot, was found to be ≈90%. Before dilution of complex for the cryo-EM grids preparation, ≈15-fold molar excess of free RRF was added in the buffer. Cryo-EM grids of the empty ribosome (control) and the ribosome–RRF complex were prepared according to the procedure described in ref. 18.

Cryo-EM and Three-Dimensional Image Reconstruction. EM data were collected on a Philips FEI (Eindhoven, The Netherlands) Tecnai F20 field emission gun electron microscope, equipped with low-dose kit and an Oxford cryo-transfer holder, at a magnification of ×50,000. A total of 48 and 76 micrographs for the control ribosomes and the ribosome–RRF complex, respectively, were scanned on a Zeiss flatbed scanner (Z/I Imaging, Huntsville, AL), with a step size of 14 μm, corresponding to 2.82 Å on the object scale. The projection-matching procedure within the SPIDER software (19) was used to obtain the three-dimensional map. We used an 11.5-Å-resolution *E. coli* 70S ribosome map (18) as the initial reference. For the control and the ribosome–RRF complex, 56,315 and 81,078 images, respec-

---

tively, were initially picked and sorted into 19 and 23 groups, respectively, according to defocus (ranging from 1.4 to 4.4 μm). Finally, only 35,156 and 51,217 images were retained, after visual and cross-correlation-based screening and removal of images from overrepresented groups among the initial set of 83 representative views of the ribosome, and these were used in the final reconstructions. The resolution of the final contrast transfer function-corrected three-dimensional maps, estimated by using the Fourier shell correlation with a cutoff value of 0.5 (see ref. 18), was 12.4 Å (or 9.1 Å by the 3σ criterion; see ref. 15) for the control, and 12.0 Å (or 8.4 Å by 3σ) for the ribosome–RRF complex. The falloff of the Fourier amplitudes toward higher spatial frequencies was corrected as described (18), using the small-angle x-ray solution scattering intensity distribution of the *E. coli* 70S ribosome.

Visualization and interpretation of the map, and docking of crystallographic structures, were performed by using SPIDER, IRIS EXPLORER (Numerical Algorithms Group, Downers Grove, IL), O (20), and RIBBONS (21). Cross-correlation coefficients (CCCs) between the fitted atomic structures of RRF and the corresponding cryo-EM density were calculated after converting atomic coordinates to EM densities and filtering them to the resolution of the cryo-EM map (see ref. 4). The accuracy of fittings of atomic structures into cryo-EM maps has been estimated to be in the range of one-tenth of the resolution of the cryo-EM map (see ref. 22), which would yield ± 1.2 Å in the case of our results with RRF.

Results and Discussion

Location of RRF on the Ribosome. The cryo-EM map of the RRF-ribosome complex shows an additional mass of density in the intersubunit space (red in Fig. 1*a*) when compared with the map of the empty ribosome (control). This extra mass is shaped as a twisted L (Fig. 1) and can be readily attributed to RRF. Along most of its length, the long arm of the L-shaped density makes contacts with the interface–canyon region of the 50S, whereas the density corresponding to the short arm is oriented toward the shoulder and the decoding region of the 30S subunit. The elbow between the two RRF domains faces the L7/L12 stalk-base and the α-sarcin–ricin loop (SRL) region of the 50S subunit. At lower threshold values, the density corresponding to the short arm extends toward the stalk-base (green in Fig. 2) of the 50S subunit. This relatively weaker density is likely due to RRF-binding-related conformational change in the RRF as well as the ribosome. It is also possible that the weaker density originates from an alternative orientation of domain II of RRF in a smaller fraction of ribosome–RRF complex (but see below).

Conformational Changes of the Ribosome. We find that the binding of RRF induces conformational changes in several locations on the ribosome. Most significant changes are observed in the immediate vicinity of RRF-binding regions (Fig. 2). The largest of the RRF-binding-related conformational changes is located between the elbow region of RRF and the L7/L12 stalk-base region of the 50S subunit. Upon RRF binding, this region of the ribosome moves toward the intersubunit space by ≈ 10 Å (Fig. 2*a*). This movement is in a direction similar to those observed previously upon binding of elongation factors (23, 24) and release factor 2 (6). The mass of density that appears (green in Fig. 2) at relatively lower density threshold setting could be associated with conformational changes in the stalk-base region, rather than being part of RRF (see below).

Other significant conformational changes involve the components of an important inter-ribosomal subunit bridge, B2a. This bridge is formed between 23S rRNA helix 69 and a top portion of 16S rRNA helix 44 (25). Both these helices move toward the tRNA exit site of the ribosome (i.e., toward the protein L1 and platform sides, respectively, of 50S and 30S subunits in Fig. 2 *b*
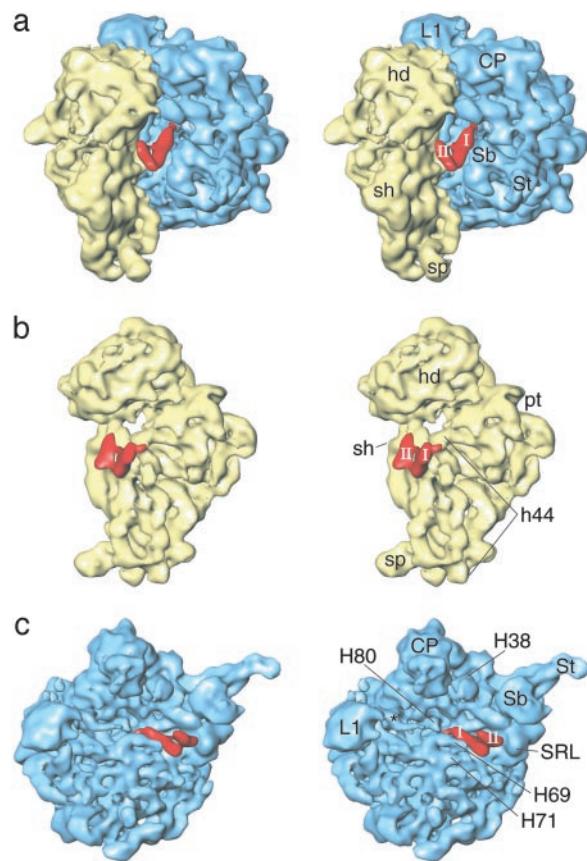

Fig. 1. Stereoview representations of the three-dimensional cryo-EM structure of the 70S ribosome–RRF complex. (*a*) 70S ribosome, showing the shoulder side of the 30S subunit (yellow) on the left, and L7/L12-stalk side of the 50S subunit (blue) on the right to reveal the binding position of RRF (red). (*b*) Computationally separated RRF density superposed onto the 30S subunit. (*c*) RRF density superposed onto the 50S subunit. hd, head; sh, shoulder; sp, spur; pt, platform; L1, L1-protein protuberance; CP, central protuberance; St, L7/L12 stalk; Sb, stalk-base; SRL, α-sarcin-ricin loop; h and H followed by numbers identify the 16S and 23S rRNA helices, respectively; I and II, domains of RRF; asterisk, density of a tRNA in the P/E state.

and *c*). Upon RRF binding, the tip of the helix 44 goes through a rotation ($\approx 18°$) around the axis of the helix and a shift (≈ 7 Å, Fig. 2*c*), which are of similar magnitudes as reported previously upon binding of EF-G (26, 27) and IF1 (2). The position of the tip of 23S rRNA helix 69 in RRF-bound and unbound maps are significantly different (Fig. 2*b*). However, fitting of the x-ray structure corresponding to helix 69 (28) does not explain such a large rigid-body shift of the whole helix 69. Because a rigid-body fit of the x-ray structure of helix 69 cannot fully account for the shifted position of the corresponding density, we believe that the absence of a portion of helix-69 density in the RRF-bound map could be partly caused by its disordered apical loop. Whereas 16S rRNA helix 44 moves away from the RRF domain II (Fig. 2*c*), 23S rRNA helix 43 moves closer to it (by ≈ 10 Å) (Fig. 2*a*).

Comparison of Atomic Structures of RRF with Corresponding cryo-EM Density. The L-shape of the RRF density in the cryo-EM map (Fig. 1) is consistent with crystal (9, 11, 13) and solution (12) structures of RRF from various species. Independent docking of all these atomic structures into the EM density shows that the density is best explained by the crystallographic structure of the *Thermotoga maritima* RRF (Fig. 3 *a* and *b*). The quality of the match between the atomic structure and the cryo-EM density was assessed by comparing the CCC values between the various
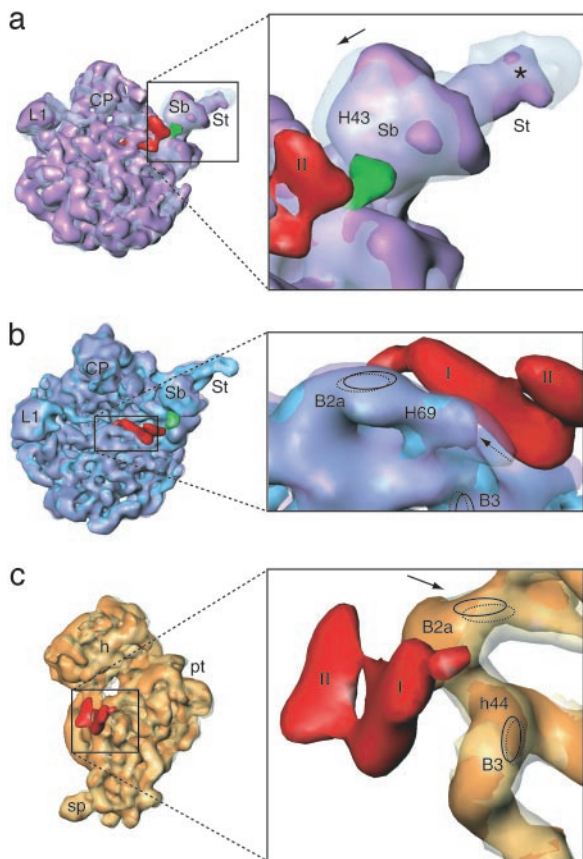
Fig. 2. Structural changes of the ribosome upon RRF binding. (*a*) Maps of RRF-bound ribosome (semitransparent blue) and the naked (control) ribosome (purple) have been superimposed. The 50S subunits are shown from the intersubunit-face side, and portions corresponding to the L7/L12 stalk-base region (Sb) and the Stalk (St) are magnified in *Inset*. Densities corresponding to RRF (red) and RRF-binding-associated conformational change (green, see text), which is visible only at lower threshold values, are also shown. (*b*) Same maps as in *a*, but transparencies have been flipped to reveal the conformational change associated with the 23S rRNA helix 69 (H69). Superimposed maps have been rotated with respect to their orientation in *a*, around a horizontal axis, by ≈35°, such that CP of the 50S subunit moves closer to the viewer. The helix 69 portion has been magnified in *Inset*. (*c*) Superimposed 30S subunits of the RRF-bound ribosome (semitransparent yellow) and naked ribosome (orange), shown from the intersubunit-face side. The helix 44 (h44) region of the 16S rRNA is magnified in *Inset*. In *b* and *c Insets*, ribosome masses from the far plane have been computationally removed for visual clarity. Arrows indicate the direction of movements of ribosomal mass upon RRF binding. Asterisk in *a* indicates a significant conformational change in the L7/L12 stalk, which becomes a more defined, thick, and extended structure upon RRF binding, as also seen previously in the case of EF-G (37). Locations of two bridges (B2a and B3) before and after RRF binding are indicated as ovals with solid and broken lines, respectively. I and II, two structural domains of RRF. All other landmarks are the same as in Fig. 1.

Fig. 3. Fitting of atomic structure of RRF into the cryo-EM density. (*a*) Stereo-view representation of the fitting of the x-ray structure of *T. maritima* RRF (domain I, pink; and domain II, violet) into the cryo-EM density (semitransparent red). In most part, the x-ray structure of RRF is embedded within the cryo-EM density, recognizable by altered hues of color for the two RRF domains (reddish pink for domain I, magenta for domain II), whereas very small portions of the x-ray structure that stick out of the cryo-EM density are visible in their original (pink or violet) colors. The cryo-EM density of RRF is shown at a lower threshold value as compared to the value used in Figs. 1 and 2. (*b*) Same as *a*, but shown from the intersubunit space side, with L7/L12 stalk facing the viewer. (*c*) Alternative fitting of RRF atomic structure (gray) into the cryo-EM map shown from the same view as in *b*. In this fitting, domain II of RRF is oriented into a weaker mass of density (semitransparent green, see text), toward the L7/L12 stalk-base region. This fitting yields a significantly lower cross-correlation value (0.51 vs. 0.77 for the fitting shown in *a* and *b*). For the purpose of comparison, only C$_\alpha$ backbones of RRF x-ray structure are shown in *b* and *c*. The orientations of the 70S ribosome (semitransparent surfaces), with RRF density (red), are shown as thumbnails on the lower right. All of the landmarks are the same as in Fig. 2.

fitted and resolution-matched atomic structures, and the cryo-EM density (Table 1). Comparison of the x-ray crystallographic structure of the *E. coli* RRF (10) with the EM density shows that domain II in the x-ray structure is in an unusually extended position, perhaps because of use of a detergent during crystallization (10). A rigid-body docking of the *E. coli* RRF x-ray structure into the cryo-EM map allows fitting of one domain at a time (i.e., when an optimum fit for domain I is obtained, a significant portion of domain II remains outside the cryo-EM density), which results in the low CCC value of 0.6 (Table 1). However, a rotation of domain II around an axis that passes through amino acid residues G30 and P104, located in the
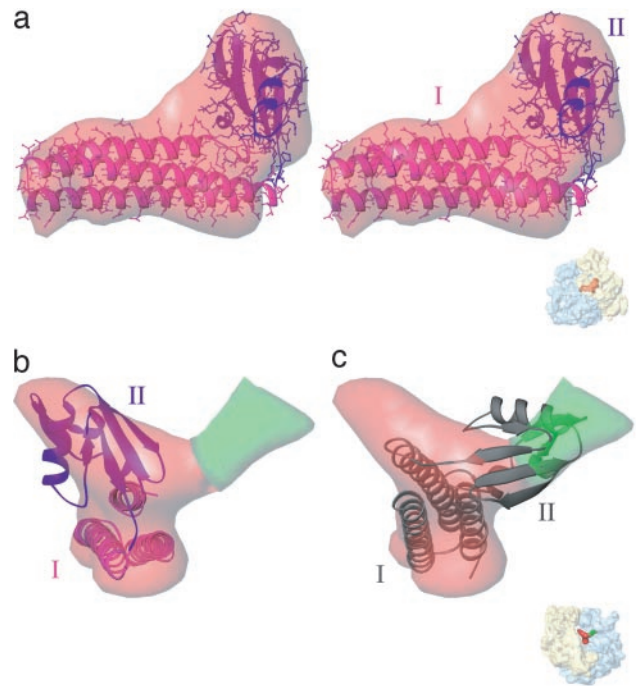
previously proposed hinge region within the elbow of the RRF (9), to match with its orientation in *T. maritima* RRF structure, results in an overall excellent fit for both structural domains of *E. coli* RRF into the EM density. The improved fit is reflected by a higher CCC value of 0.79 (Table 1).

We also explored an alternative rigid-body fit for all five atomic structures, in which domain II was oriented toward the stalk base of the 50S, taking into account the previously mentioned weaker mass of density (green mass in Figs. 2 and 3). For a comparison between two fits shown in Fig. 3 *b* and *c*, one should compare CCC values in the second and fourth columns, respectively, of Table 1. Because the alternative fits invariably produced a significantly lower CCC values (fourth and fifth columns vs. second and third columns, respectively), we believe that this orientation of domain II is unlikely. Therefore, henceforth, we discuss our results based on the orientation of RRF (Fig. 3 *a* and *b*) that yields the highest CCC value.

Interaction Sites Between RRF and the Ribosome. In RRF, the α-helix 5 (see ref. 9) segment, encompassing amino acid residues 122–133 within domain I, together with its immediate neighbors on the α-helical bundle, helix 6, encompassing amino acid

Table 1. CCC values of fits between atomic structures of RRF from various species and the corresponding cryo-EM density

Atomic structure organism (PDB ID)	Rigid-body fit*	Two domains fitted separately†	Rigid-body fit in the alternative position‡	Two domains fitted separately in the alternative position§
E. coli (1EK8)	0.60	0.79¶	0.42	0.61
T. maritima (1DD5)	0.77	0.77	0.51	0.56
Thermus thermophilus (1EH1)	0.74	0.73	0.53	0.56
Aquifex aeolicus (1GE9)	0.73	0.74	0.57	0.59
Vibrio parahaemolyticus (1IS1)	0.74	0.75	0.59	0.60

*RRF atomic structure was fitted as one rigid body, as shown in Fig. 3 *a* and *b*.

†Two domains of RRF were fitted separately as two rigid bodies, in an overall orientation similar to that shown in Fig. 3 *a* and *b*.

‡RRF atomic structure was fitted as one rigid body in an alternative position, taking the weaker mass of density into account, as shown in Fig. 3*c*.

§Two domains of RRF were fitted separately as two rigid bodies, in an overall orientation similar to that shown in Fig. 3*c*.

¶When two *E. coli* RRF domains were aligned according to their orientations in *T. maritima* atomic structure. All contacts of RRF with the ribosome were analyzed according to this fit.

residues 161–165 (Fig. 4*a*), appear to form the most stable connection with the ribosome, as the corresponding cryo-EM density remains visible at very high-density threshold values. It is likely that the corresponding portion of RRF constitutes the main ribosome-anchoring site.

Most of the contacts that are made between RRF domain I and the ribosome involve certain modified 23S rRNA bases, which either interact directly with RRF, or are present in the immediate vicinity of this factor. The amino acid residue E150, present near the tip of RRF domain I, makes contact with
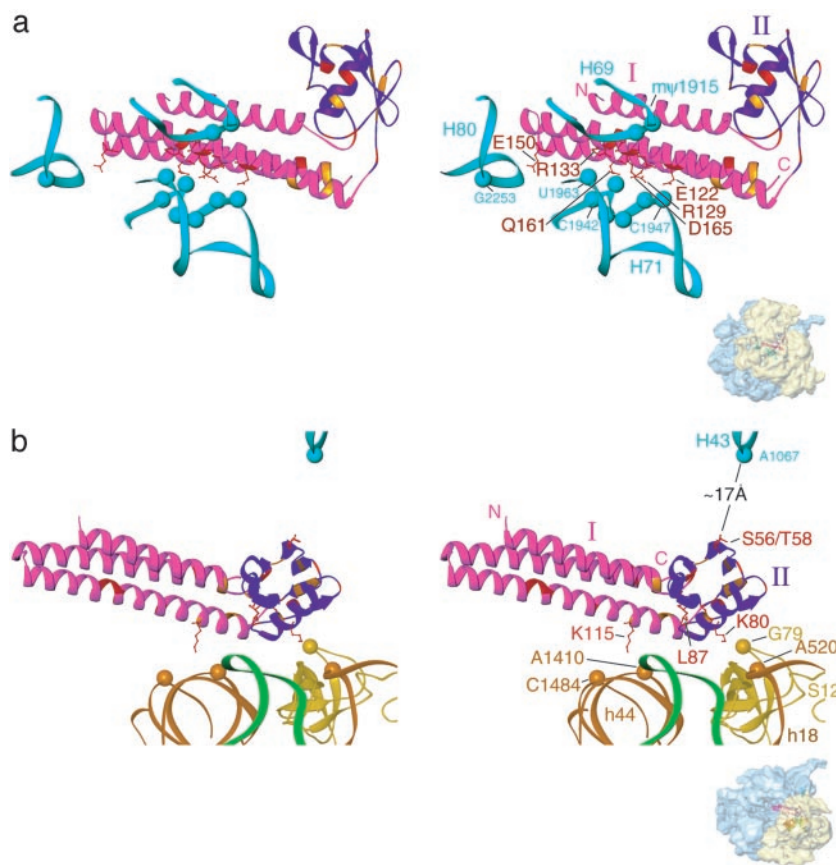

Fig. 4. Sites of interaction between RRF and ribosome. X-ray crystallographic structures of both ribosomal subunits (28, 41) were fitted into the cryo-EM map of the RRF-ribosome complex. (*a*) The 23S rRNA helices (light blue) of the 50S ribosome that directly interact with (or lie within 3 Å of) RRF are shown. Domains I (magenta) and II (purple) of the RRF atomic structure are assigned the same colors as in Fig. 3 *a* and *b*, with conserved (red) and semiconserved (orange) residues highlighted. The RRF residues making direct contact with rRNA are shown with side chains (red). Ribosomal RNA residues making direct contacts with RRF are highlighted as beads in corresponding color. (*b*) Regions of ribosome that lie within 5–10 Å distant [except for helix 43 (H43) of the 23S rRNA, see below], and the position of a segment of mRNA (green, ref. 40). Relevant segments of 16S rRNA helices 18 and 44 (brown) and protein S12 (yellow) are shown. Note that residue A1067 of H43 is well within the reach ($\approx$17 Å) of the HR probe site, S56, of RRF (ref. 14; also see supporting information). The orientation of the 70S ribosome is shown as a thumbnail on the lower right. Only some of the relevant amino acid residues of RRF and nucleotide residues of rRNA are identified. All other landmarks are the same as introduced in Figs. 1–3.

nucleotide G2253 within the apical loop of the 23S rRNA helix 80 (Fig. 4a). Our map indicates a conformational change in the tip region of helix 80 (not shown), which likely involves the neighboring methylated base G2251 in this interaction. It should be noted that the G2253 is also known to interact with the CCA-end of the peptidyl–tRNA in the P site (29). In the posttermination complex, the CCA-end of tRNA is already in the E site because it has released the peptidyl group with the help of release factor 1 or 2. Because RRF competes with N-acetyl phenylalanyl tRNA for the P-site (30) in the posttermination complex, it is conceivable that the absence of the CCA end of the P-site tRNA is a prerequisite for RRF binding.

Based on the rigid-body fits of both RRF domains (i.e., without considering any intradomain rearrangements), we have identified certain amino acid residues of RRF that make contact with specific residues of the rRNAs. Highly conserved amino acid residues of RRF, E122–R133, interact with helix 69 of the 23S rRNA. Amino acid residues E122 and V126 make direct contacts with methyl-pseudouridine at position 1915, whereas V130 contacts an adenine residue at position 1916 (shown as a blue ball next to residue 1915) of the rRNA helix 69 (Fig. 4a), with another pseudouridine present in the immediately adjacent position, 1917. Helix 71 of the 23S rRNA also makes tight contacts with the most conserved amino acid segment (E122–R133) of RRF: rRNA residues U1946 and C1947 with E122, G1945 with a highly conserved R129, and U1963 with R133; whereas the universally conserved neighboring amino acid residue, R132, lies within a van der Waals interaction distance of U1963. Helix 71 makes additional contacts with a segment of amino acid residues (Q161 and D165) on the C-terminal α-helix within domain I: C1941 with Q161, and U1943 and U1944 with D165. Again, the rRNA residues in the close neighborhoods of these contacts are modified bases, methyl-U1939 and methyl-C1962. Observation of an interaction of RRF, involving its C terminus, is consistent with genetic studies (31, 32) showing that this region of RRF is important for its occupancy on the ribosome.

Although no direct interaction with the 30S subunit is visible in the map, the possibility of an involvement of 16S rRNA helix 18 and protein S12, both of which lie within 6–8 Å of RRF, and 16S rRNA helix 44, which lies within 7–10 Å of RRF, cannot be ruled out. As a matter of fact, helix 44 moves upon RRF binding (Fig. 2c).

Although the overall location of RRF derived in our cryo-EM study appears similar to that obtained from an interpretation of the HRP data (14), the orientations of the RRF domains in the two studies are significantly different. For example, in our study, RRF domain II is oriented toward the 30S subunit (Fig. 1a) as compared to its orientation derived from the interpretation of HRP data (14). In addition, RRF in our study is situated more (by ≈5 Å) inside the intersubunit space, and oriented such that tip of its domain I is shifted more toward protein L5 within the central protuberance (by ≈13 Å; see supporting information, which is published on the PNAS web site) of the 50S subunit. However, our results satisfy most of the data obtained with the HRP (see supporting information), i.e., probed amino acid residues of RRF and target rRNA residues fall within the allowed range (20–50 Å) of the HR probe. If we place RRF according to the alternative fit (Fig. 3c), which invariably produces a significantly lower CCC values (Table 1, fourth and fifth columns vs. second and third columns, respectively), domain II would occupy an intermediate position between its positions derived from the HRP study (14) and the present study (Fig. 3b, also see supporting information).

Binding Position with Respect to the Binding Sites of tRNAs and EF-G.
RRF interacts with the ribosome in a functional state with empty A and P sites on the 50S subunit, but with a deacylated tRNA
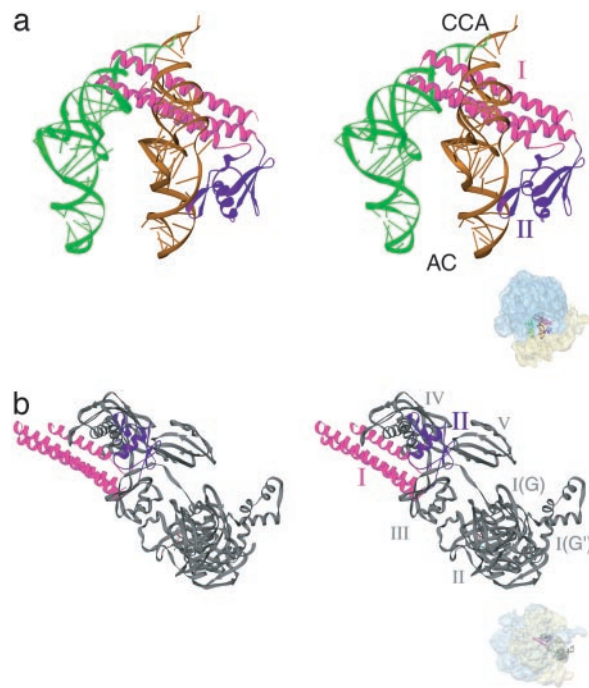

Fig. 5. Stereo representation of relative binding position of RRF with respect to tRNAs and EF-G on the ribosome. (a) With respect to the A- (orange) and P- (green) site tRNAs. (b) With respect to EF-G (gray) in the GDP state. CCA, CCA-end side of the tRNAs; AC, anticodon side of the tRNAs; domains I and II of RRF and domains I–V of EF-G are denoted in respective matching colors. Orientations of the 70S ribosome in the two panels are represented by thumbnails at the lower right. In a, the 30S subunit is situated below the 50S subunit such that head of the 30S subunit and the CP of the 50S subunit face the viewer, whereas in b, the solvent side of the 30S subunit faces the viewer.

expected to be present in an intermediary P/E position (14). Comparison of the RRF-binding position with previously determined positions of tRNAs (25, 33) shows that the upper half of domain I of RRF overlaps with the CCA arms of the A- and P-site tRNAs, whereas the tip of RRF domain II partially overlaps with the anticodon arm of the A-site tRNA (Fig. 5a). This observation is in line with inferences drawn from previous biochemical studies, which indicate that RRF occupies both the A (30, 34) and P (30) sites. In our map, we see a strongly bound tRNA (density marked by an asterisk in Fig. 1c) in a P/E position (ref. 35; also see supporting information), indicating that RRF does not compete for this site in its initial binding on the ribosome (14, 16). We have also obtained a preliminary cryo-EM map of a complex of RRF with puromycin-treated polysomes, a natural substrate for RRF binding, which shows the same binding position of RRF (M.R.S., C. Barat, S. Raj, A.K., and R.K.A., unpublished data), as obtained in the present study.

The fact that RRF works in concert with EF-G has been established (8, 36). Our analysis shows that RRF and EF-G share overlapping binding positions on the ribosome (Fig. 5b). The elbow of RRF is found in an overlapping position at the junction of domains III, IV, and V of EF-G (23, 37), whereas RRF domain II occupies an overlapping position with domain IV in the GDP state of EF-G (Fig. 5b). Even though RRF has a structure and dimension similar to a tRNA (9), its orientation on the ribosome is strikingly different from those of tRNA and tRNA-mimicking domains of EF-G, indicating that the direct molecular-mimicry hypothesis (9) is not tenable for RRF. However, the fact that RRF is moved by EF-G (16) before it releases mRNA strongly suggests a conceptual similarity between EF-G-dependent movements of RRF and tRNAs on the ribosome.

Clearly, the steric clash between the binding position of RRF and EF-G (Fig. 5b) implies that the binding of EF-G must move RRF toward the E site (16, 17). As domains III–V of EF-G acquire proper binding positions on the ribosome (37), RRF will be pushed toward the E-site region to eject the tRNA from the ribosome.

RRF forms its strongest interactions with the 23S rRNA helices 69 and 71 (Fig. 4a). These helices participate in the formation of the two most prominent and conserved intersubunit bridges, B2a and B3, respectively (25). Direct interaction of RRF with these bridges, which appear to shift upon RRF binding (Fig. 2 b and c), could be responsible for the dissociation of the subunits under certain conditions (38). As mentioned earlier, these interactions also involve modified nucleotides of the 23S rRNA, which are likely to make these interactions stronger (ref. 39 and Jim Ofengand, personal communication). Furthermore, helix 69 of the 23S rRNA is the only component of the 50S subunit that makes contact with RRF and interacts with the decoding site within helix 44 of the 16S rRNA, the site that harbors a part of the ribosome-bound mRNA (40) and moves by ≈7 Å upon RRF binding (Fig. 2c). It is therefore conceivable that any strain exerted on these relatively strong ribosome–RRF interactions by subsequent movement and release of RRF by EF-G will also disrupt the mRNA binding, and this disruption could be instrumental in the release of mRNA from the post-termination complex.

1. McCutcheon, J. P., Agrawal, R. K., Philips, S. M., Grassucci, R. A., Gerchman, S. E., Clemons, W. M., Jr., Ramakrishnan, V. & Frank, J. (1999) *Proc. Natl. Acad. Sci. USA* **96,** 4301–4306.
2. Carter, A. P., Clemons, W. M., Jr., Brodersen, D. E., Morgan-Warren, R. J., Hartsch, T., Wimberly, B. T. & Ramakrishnan, V. (2001) *Science* **291,** 498–501.
3. Stark, H., Rodnina, M. V., Rinke-Appel, J., Brimacombe, R., Wintermeyer, W. & van Heel, M. (1997) *Nature* **389,** 403–406.
4. Agrawal, R. K., Penczek, P., Grassucci, R. A. & Frank, J. (1998) *Proc. Natl. Acad. Sci. USA* **95,** 6134–6138.
5. Klaholz, B. P., Pape, T., Zavialov, A. V., Myasnikov, A. G., Orlova, E. V., Vestergaard, B., Ehrenberg, M. & van Heel, M. (2003) *Nature* **421,** 90–94.
6. Rawat, U. B., Zavialov, A. V., Sengupta, J., Valle, M., Grassucci, R. A., Linde, J., Vestergaard, B., Ehrenberg, M. & Frank, J. (2003) *Nature* **421,** 87–90.
7. Klaholz, B. P., Myasnikov, A. G. & van Heel, M. (2004) *Nature* **427,** 862–865.
8. Kaji, A., Kiel, M. C., Hirokawa, G., Muto, A. R., Inokuchi, Y. & Kaji, H. (2001) *Cold Spring Harbor Symp. Quant. Biol.* **66,** 515–529.
9. Selmer, M., Al-Karadaghi, S., Hirokawa, G., Kaji, A. & Liljas, A. (1999) *Science* **286,** 2349–2352.
10. Kim, K. K., Min, K. & Suh, S. W. (2000) *EMBO J.* **19,** 2362–2370.
11. Toyoda, T., Tin, O. F., Ito, K., Fujiwara, T., Kumasaka, T., Yamamoto, M., Garber, M. B. & Nakamura, Y. (2000) *RNA* **6,** 1432–1444.
12. Yoshida, T., Uchiyama, S., Nakano, H., Kashimori, H., Kijima, H., Ohshima, T., Saihara, Y., Ishino, T., Shimahara, H., Yoshida, T., *et al.* (2001) *Biochemistry* **40,** 2387–2396.
13. Nakano, H., Yoshida, T., Uchiyama, S., Kawachi, M., Matsuo, H., Kato, T., Ohshima, A., Yamaichi, Y., Honda, T., Kato, H., *et al.* (2003) *J. Biol. Chem.* **278,** 3427–3436.
14. Lancaster, L., Kiel, M. C., Kaji, A. & Noller, H. F. (2002) *Cell* **111,** 129–140.
15. Orlova, E. V., Dube, P., Harris, J. R., Beckman, E., Zemlin, F., Markl, J. & van Heel, M. (1997) *J. Mol. Biol.* **271,** 417–437.
16. Hirokawa, G., Kiel, M. C., Muto, A., Selmer, M., Raj, V. S., Liljas, A., Igarashi, K., Kaji, H. & Kaji, A. (2002) *EMBO J.* **21,** 2272–2281.
17. Kiel, M. C., Raj, V. S., Kaji, H. & Kaji, A. (2003) *J. Biol. Chem.* **278,** 48041–48050.
18. Gabashvili, I. S., Agrawal, R. K., Spahn, C. M., Grassucci, R. A., Svergun, D. I., Frank, J. & Penczek, P. (2000) *Cell* **100,** 537–549.
19. Frank, J., Penczek, P., Agrawal, R. K., Grassucci, R. A. & Heagle, A. B. (2000) *Methods Enzymol.* **317,** 276–291.
20. Jones, T. A., Zou, J. Y., Cowan, S. W. & Kjeldgaard (1991) *Acta Crystallogr. A* **47,** 110–119.

21. Carson, M. (1991) *J. Appl. Crystallogr.* **24,** 103–106.
22. Rossmann, M. G. (2000) *Acta Crystallogr. D* **56,** 1341–1349.
23. Agrawal, R. K., Linde, J., Sengupta, J., Nierhaus, K. H. & Frank, J. (2001) *J. Mol. Biol.* **311,** 777–787.
24. Valle, M., Zavialov, A., Li, W., Stagg, S. M., Sengupta, J., Nielsen, R. C., Nissen, P., Harvey, S. C., Ehrenberg, M. & Frank, J. (2003) *Nat. Struct. Biol.* **10,** 899–906.
25. Yusupov, M. M., Yusupova, G. Z., Baucom, A., Lieberman, K., Earnest, T. N., Cate, J. H. & Noller, H. F. (2001) *Science* **292,** 883–896.
26. Frank, J. & Agrawal, R. K. (2000) *Nature* **406,** 318–322.
27. VanLoock, M. S., Agrawal, R. K., Gabashvili, I. S., Qi, L., Frank, J. & Harvey, S. C. (2000) *J. Mol. Biol.* **304,** 507–515.
28. Harms, J., Schluenzen, F., Zarivach, R., Bashan, A., Gat, S., Agmon, I., Bartels, H., Franceschi, F. & Yonath, A. (2001) *Cell* **107,** 679–688.
29. Moazed, D. & Noller, H. F. (1989) *Cell* **57,** 585–597.
30. Hirokawa, G., Kiel, M. C., Muto, A., Kawai, G., Igarashi, K., Kaji, H. & Kaji, A. (2002) *J. Biol. Chem.* **277,** 35847–35852.
31. Janosi, L., Mottagui-Tabar, S., Isaksson, L. A., Sekine, Y., Ohtsubo, E., Zhang, S., Goon, S., Nelken, S., Shuda, M. & Kaji, A. (1998) *EMBO J.* **17,** 1141–1151.
32. Rao, A. R. & Varshney, U. (2002) *Microbiology* **148,** 3913–3920.
33. Agrawal, R. K., Spahn, C. M., Penczek, P., Grassucci, R. A., Nierhaus, K. H. & Frank, J. (2000) *J. Cell Biol.* **150,** 447–459.
34. Pavlov, M. Y., Freistroffer, D. V., Heurgue-Hamard, V., Buckingham, R. H. & Ehrenberg, M. (1997) *J. Mol. Biol.* **273,** 389–401.
35. Agrawal, R. K., Penczek, P., Grassucci, R. A., Burkhardt, N., Nierhaus, K. H. & Frank, J. (1999) *J. Biol. Chem.* **274,** 8723–8729.
36. Rao, A. R. & Varshney, U. (2001) *EMBO J.* **20,** 2977–2986.
37. Agrawal, R. K., Heagle, A. B., Penczek, P., Grassucci, R. A. & Frank, J. (1999) *Nat. Struct. Biol.* **6,** 643–647.
38. Karimi, R., Pavlov, M. Y., Buckingham, R. H. & Ehrenberg, M. (1999) *Mol. Cell* **3,** 601–609.
39. Ofengand, J., Malhotra, A., Remme, J., Gutgsell, N. S., Del Campo, M., Jean-Charles, S., Peil, L. & Kaya, Y. (2001) *Cold Spring Harbor Symp. Quant. Biol.* **66,** 147–159.
40. Yusupova, G. Z., Yusupov, M. M., Cate, J. H. & Noller, H. F. (2001) *Cell* **106,** 233–241.
41. Wimberly, B. T., Brodersen, D. E., Clemons, W. M., Jr., Morgan-Warren, R. J., Carter, A. P., Vonrhein, C., Hartsch, T. & Ramakrishnan, V. (2000) *Nature* **407,** 327–339.

BIOCHEMISTRY